Journal of Photochemistry and Photobiology A: Chemistry 224 (2011) 8–15

Contents lists available at SciVerse ScienceDirect

Journal of Photochemistry and Photobiology A: Chemistry

journal homepage: www.elsevier.com/locate/jphotochem

Dry photochemical synthesis of hydrotalcite, γ-Al_2O_3 and TiO_2 supported gold nanoparticle catalysts

Geniece L. Hallett-Tapley[a], Charles-Oneil L. Crites[a], María González-Béjar[a], Katherine L. McGilvray[a], José Carlos Netto-Ferreira[a,b,*], J.C. Scaiano[a,**]

[a] Centre for Catalysis Research and Innovation, Department of Chemistry, University of Ottawa, 10 Marie Curie, Ottawa K1N 6N5, Canada
[b] Departamento de Química, Universidad Federal Rural do Rio de Janeiro, Seropédica, 23851-970 Rio de Janeiro, Brazil

ARTICLE INFO

Article history:
Received 1 May 2011
Received in revised form 13 August 2011
Accepted 18 August 2011
Available online 8 September 2011

Keywords:
Photochemistry
Gold nanoparticles
Hydrotalcite
Al_2O_3
TiO_2
Catalysis

ABSTRACT

Gold nanoparticles (AuNP) supported on hydrotalcite, γ-Al_2O_3 and TiO_2 P25 have been prepared photochemically under mild conditions using ketyl radicals as the primary reducing agent; these nanocomposites were prepared directly in the solid phase. Such dry, solventless methods are attractive from an environmental perspective. The composite materials were successfully characterized using diffuse reflectance UV–visible spectroscopy, SEM, TEM, X-ray diffraction spectroscopy (XRD) and X-ray photoelectron spectroscopy (XPS). The supported AuNP were predominantly spherical and ranged in size from 20–140 nm depending on the support and the percent Au loading, indicating the potential applications of these particles as photocatalysts. The catalytic activity of the supported AuNP was evaluated using the well-studied reduction of 4-nitrophenol. UV–visible spectroscopy was used to monitor the reaction and illustrated the ability of these easily prepared AuNP composites to act has heterogeneous catalysts. The role of percent Au loading and type of support on the catalytic activity of supported AuNP was also investigated. Composites with relatively large AuNP may hold promise as efficient catalysts in plasmon-mediated light-driven reactions.

1. Introduction

Considerable attention has been placed on the generation of diverse noble metal nanoparticles due to the prospective applications in areas of bioscience, diagnostic imaging [1], and in organic chemistry [2,3], particularly in the field of catalysis [4–6]. Metallic gold had long been considered to be catalytically inert, until nanoscale preparations of colloidal gold exploited the catalytic potential of these materials, leading to a resurgence of research on gold catalysts [4,7,8]. Current interests concentrate on supported noble metal nanoparticles due to their potential as heterogeneous catalysts [5]. The use of gold nanoparticle (AuNP) composites in catalysis presents several advantages. The first focuses on the ability of the solid support to stabilize small AuNP and, thus, minimize nanoparticle aggregation, crucial towards conserving the catalytic properties of the nanomaterial composites [5]. Further, the support is believed to participate in the reaction by contributing to catalytic cycling [5,9]. Strong interactions between the support and the AuNP are believed to account for changes in catalytic activity of AuNP on various solid supports. The support can be an integral part of the reaction pathway, allowing for different outcomes depending on the irradiation wavelength [10]. In addition, supported nanoparticles can be readily separated from reagents and products (in contrast with colloidal suspensions).

Supported AuNP have also gained recognition as potentially environmentally friendly catalysts [11], which can be developed at minimal cost and have been shown to cleanly catalyze various organic reactions, such as CO oxidation [4,7,12], alcohol oxidation [13–17] and olefin epoxidation [16], as effectively as harsh chemicals frequently employed for these reactions.

Supported AuNP have been prepared using a variety of techniques, with most focusing on the direct adsorption of the gold precursor onto the support followed by thermal or chemical reduction [5,6,16,18]. Recent reports from our laboratory have shown that aqueous AuNP can be prepared photochemically from $HAuCl_4$ and the benzoin Irgacure 2959 (I-2959) under mild conditions [19–22]. Following UVA irradiation of I-2959, 2-hydroxy-2-propyl (ketyl) radicals are generated *via* rapid Norrish Type I α-cleavage and reduce Au^{3+} to Au^0 (Scheme 1). The implementation of photochemical methods allows for spatial and temporal control throughout the growth process by varying the intensity and duration of UVA irradiation [20]. The photochemical synthesis of supported AuNP presents several distinct advantages as a green

* Corresponding author at: Centre for Catalysis Research and Innovation, Department of Chemistry, University of Ottawa, 10 Marie Curie, Ottawa K1N 6N5, Canada.
** Corresponding author. Tel.: +1 613 562 5896; fax: +1 613 562 5633.
E-mail addresses: josecarlos@photo.chem.uottawa.ca (J.C. Netto-Ferreira), tito@photo.chem.uottawa.ca, titoscaiano@mac.com (J.C. Scaiano).

1010-6030/$ – see front matter © 2011 Published by Elsevier B.V.
doi:10.1016/j.jphotochem.2011.08.013

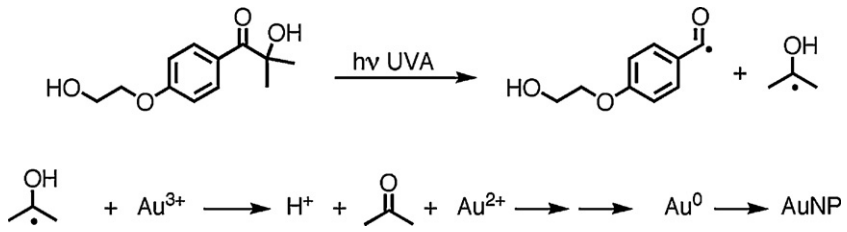

Scheme 1. Generation of AuNP *via* Norrish Type I photocleavage of the I-2959 ketyl radical precursor.

alternative [23] by employing light as an initiator. Primarily, the use of toxic chemicals and/or high temperatures can be minimized, thus providing a more environmentally friendly route for the preparation of these materials. Further, the absence of co-added stabilizing agents coupled with the use of Soxhlet extraction allows for the removal of secondary photochemical byproducts from the nanoparticle surface, exposing a larger surface area for catalysis. Though such a method cannot be termed as strictly solventless, the minimal amounts of acetonitrile used in both the preparation and washing stages of these composites could be easily recycled, a favourable alterative [24] to the large amounts of water required to wash similar catalysts prepared *via* chemical reduction. Moreover, the ease of catalyst removal following reaction is a desireable and an attractive advantage.

In this work we have applied a dry photochemical approach to make supported AuNP. Initial adsorption of the $HAuCl_4$ and the free radical precursor, I-2959, onto the support, followed by UVA irradiation of the material led to the efficient generation of supported AuNP.

2. Experimental

2.1. Reagents

All materials were used as received, unless otherwise indicated. Gold (III) tetrachloroauric acid hydrate ($HAuCl_4{\cdot}3H_2O$), hydrotalcite (HT), 4-nitrophenol, 4-aminophenol and sodium borohydride ($NaBH_4$) were purchased from Sigma–Aldrich. γ-Aluminum oxide (γ-Al_2O_3) was purchased from BDH Chemicals. TiO_2 P25 was a gift from Evonik Degussa. Irgacure-2959 (I-2959) was a gift from Ciba Specialty Chemicals and was recrystallized twice from ethyl acetate. Optima grade CH_3CN was purchased from Fisher Chemicals and was used in all cases. Millipore H_2O (resistivity 18.2 MΩ at 25 °C) was deionized in house and was used for all catalyst screening experiments.

2.2. Instruments

Solid state irradiation to induce NP formation was performed using 5 UVA bulbs and a Luzchem EXPO panel (see set up photograph in Supplementary Information). The intensity in the UVA region was determined to be 65 W/m^2 using a Luzchem SPR-4001 spectroradiometer. Diffuse reflectance spectra were recorded using a Cary 1 spectrometer using a diffuse reflectance accessory. The dimensions of the supported AuNP were determined using a JSM-7500F field emission scanning electron microscope (SEM) from JEOL Ltd. The use of solid samples limited the ability of the electron beam to efficiently penetrate the sample, therefore a backscattering detector was used that allowed for easier visual detection of the nanoparticles. Using the backscattering detector, metallic elements are brighter on the image than those of non-metallic nature (i.e., supports). For the size distribution histograms and average AuNP size, 150–200 particle measurements were taken. Transmission electron microphotographs (TEM) were collected using a field emission JEM-2100F FTEM. X-ray diffraction (XRD) was recorded using a Siemens D5000 XRD diffractometer with Cu Kα X-rays (λ = 1.5418 Å). X-ray photoelectron spectroscopy (XPS) was recorded using Kratos analytical model Axis Ultra DLD, using monochromatic aluminum Kα X-rays at a power of 140 W.

UV–visible absorption spectra and kinetics for the AuNP catalyzed reduction of 4-nitrophenol were recorded on a Cary 50 spectrometer using the scanning kinetic function. UV–visible spectra were collected as a function of time to allow for a kinetic overview of the reaction system. Spectra were recorded between 250 nm and 500 nm and the time delay between spectra was dependant upon the support used, however was extended until the reaction had reached completion (between 15 and 60 min).

2.3. Synthesis of supported Au nanoparticles

0.1 mmol of $HAuCl_4$ and 0.3 mmol of I-2959 were dissolved in 60 mL HPLC grade CH_3CN followed by the addition of 1 g of the solid support. The slurry was stirred for 2–3 h to allow for Au source and I-2959 adsorption onto the support surface. The mixture was then treated under high vacuum and the remaining solid placed in glass vials and irradiated using an exposure panel from Luzchem Research equipped with 5 UVA bulbs (65 W/m^2). The exposure panel was fitted above a modified hotdog cooker with the heating element disabled (Waring PRO Professional Hotdog Griller, Model HDG100C). This simple setup was used to continuously rotate the powder samples during irradiation to ensure the homogeneous irradiation of the samples. Irradiation times varied with the support used. Au supported on HT was irradiated for 12 h and Au supported on γ-Al_2O_3 and TiO_2 P25 for 8 h. The AuNP composites were thoroughly washed by Soxhlet extraction for 48–72 h using CH_3CN as the extraction solvent to remove any unreacted $HAuCl_4$, organic photoproducts or unsupported AuNP. The solvent from the synthesis and extraction could be readily recovered.

2.4. Supported AuNP catalysis of 4-nitrophenolate reduction

Catalyst testing was performed in a 3 mL quartz cuvette (1 cm × 1 cm). 1–2 mg of catalyst was added to 2.8 mL of MilliQ water and sonicated of 10–15 s; 100 μL of a 1.1 M $NaBH_4$ solution was added to the catalyst/water suspension followed by the rapid addition of 100 μL of an aqueous 4-nitrophenol solution (3.76×10^{-3} M), immediately before monitoring the reaction *via* UV–visible spectroscopy.

3. Results and discussion

3.1. Photochemical generation and characterization of supported AuNP

The generation of Au nanoparticles on hydrotalcite (HT), γ-Al_2O_3 and TiO_2 P25 was adapted from our previous work in solution [19,20]. In all cases, a 1% or 5% nominal Au loading by weight of the solid support and a molar ratio of I-2959 to Au(III) of 3:1 was used. A detailed description of the synthesis procedure can be found in Section 2. Briefly, solid, dry samples (following liquid phase

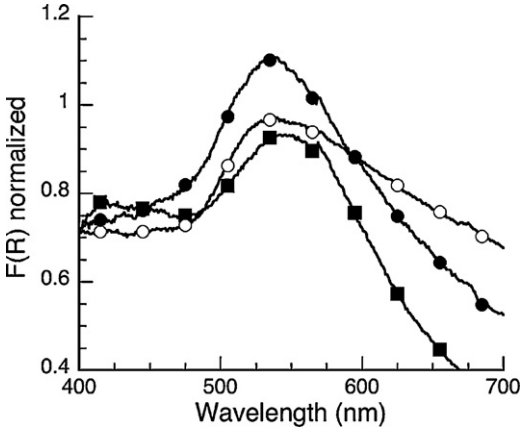

Fig. 1. Diffuse reflectance spectra of 1% Au on HT (●), on γ-Al_2O_3 (○) and on TiO_2 P25 (■); the spectra for the support blanks have been subtracted.

deposition of the reagents on the support) were irradiated from the top, while the horizontal sample tubes were rotated (3 rpm) in a modified hot dog cooker. This inexpensive arrangement (see Supplementary Data) proved a remarkably efficient way of ensuring that all surfaces of the solid powder were exposed. In fact, it is rather remarkable that this process works so well, considering that it requires diffusion of the reagents on the surface, as well as migration of gold atoms or small clusters to form the AuNP (see Scheme 1).

Typically, AuNP formation is confirmed by a visible change in colour, with the colour of spherical AuNP varying from pink to blue, depending on the degree of nanoparticle aggregation [1,19,22,25]. Furthermore, UV–visible spectroscopy of the surface plasmon band (SPB) can be used as a reporter for the formation and size of the nanoparticles as described by Mie [26] (λ_{max} = 520 nm for AuNP ~ 15 nm in size) [19,25]. The absorption maximum of the SPB can be modified by NP size, with the overall absorption of larger or more aggregated particles being red-shifted [19,22,25]. However, the SPB can also be largely influenced by the dielectric constant of the supporting matrix, where supports with higher dielectric constants have red shifted SPB absorptions [27,28]. AuNP generation was identified by the formation of a violet solid throughout the course of irradiation, attributed to the surface plasmon resonance of the AuNP composite. Diffuse reflectance spectra of AuNP on HT, γ-Al_2O_3 and TiO_2 P25 are presented in Fig. 1. Specifically, the SPB λ_{max} are observed at 533 nm for 1% Au/HT, 537 nm for 1% Au/γ-Al_2O_3 and 542 nm for 1% Au/TiO_2 P25. All three absorptions are comparable to the absorption of aqueous AuNP prepared using our photochemical synthesis and indicate that ketyl radical are sufficiently mobile on solid supports to reduce Au^{3+} [19,20].

As expected, the SPB absorptions varied depending upon the type of solid support and were considerably broader than those in solution [29]. The red-shift in the λ_{max} values on going from HT to γ-Al_2O_3 to TiO_2 P25 can be used to initially access the average size of the AuNP adsorbed onto the surface of these solids. AuNP adsorbed onto HT have the more blue-shifted SPB, indicating the smallest AuNP of the three supports presented here [19]. However, the evident bathochromic shifting of the SPB absorptions on going from HT to TiO_2 P25 may also be a reflection of the dielectric constants of the supporting medium with these values varying from ~8.6 for HT, to 9 for Al_2O_3 and 86 for TiO_2 [30]. Therefore, both NP size and the dielectric constants of the inorganic supports may play integral roles in the increasing λ_{max} of the SPB on varying the support from HT to TiO_2.

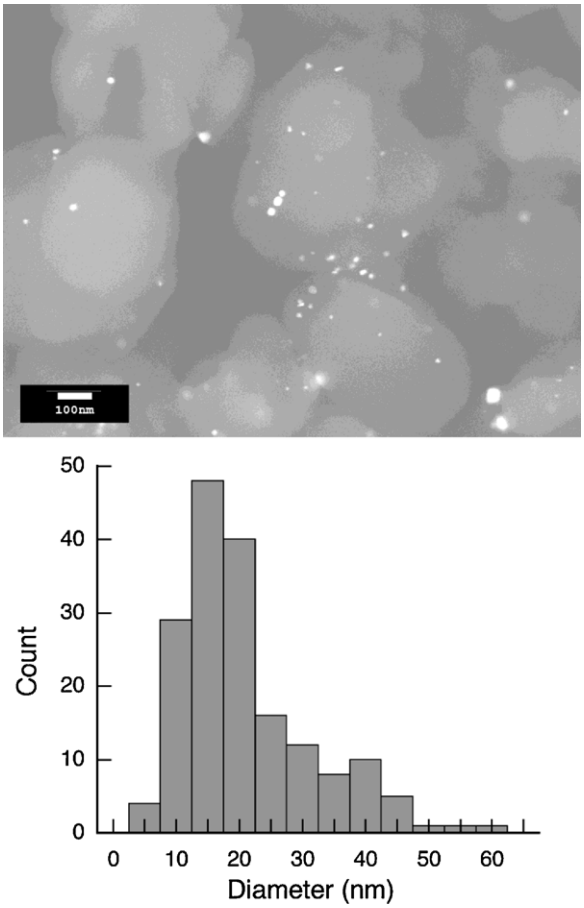

Fig. 2. SEM image for 1% Au on HT (top) and the size distribution histogram (bottom) used to access the average particle size of this AuNP composite.

3.2. SEM and TEM imaging

Particle size and morphology was further characterized through the use of SEM and TEM imaging techniques. SEM was used to determine the average size of the supported AuNP prepared with 1% loading. In all cases, the AuNP were predominantly spherical, but showed larger polydispersity than typically observed in solution [19,20,22]. The average size of the supported AuNP (1% wt) was 21 nm for HT, 30 nm for γ-Al_2O_3 and 33 nm for TiO_2 P25. Fig. 2 presents the SEM image of 1% Au/HT accompanied by the size distribution histogram. In the presented SEM images, the grey areas are indicative of support surface and bright, circular areas are representative of metallic species. The size and morphology of the particles on less dense regions of the supports was further validated using higher resolution TEM, as shown in Fig. 3. The observed particle size and polydispersity detailed from the electron microscopy analysis (Table 1) are in good agreement with the diffuse reflectance spectra.

Table 1
Average size and polydispersity (PDI) of the supported AuNP prepared in this work.

Support	% Au loading (nominal)	Ave. NP size (nm)	PDI
HT	1	21	1.24
	5	47	1.31
γ-Al_2O_3	1	30	1.14
	5	112	1.22
TiO_2 P25	1	33	1.20
	5	142	1.26

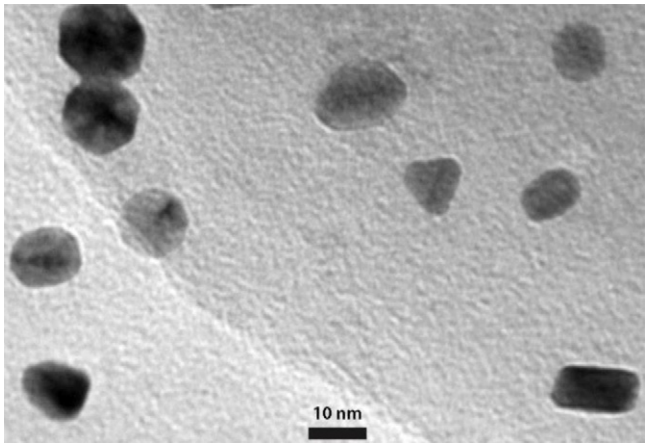

Fig. 3. TEM image for 1% Au supported on HT.

From the imaging techniques employed in this work, HT tends to be the better support for small AuNP formation, followed by γ-Al_2O_3 and TiO_2 P25. The polydispersity of the AuNP size is also dependent on the supporting structure. A comparison between 1% Au loaded composites shows that though the generated nanoparticles on HT have an overall smaller average size, the polydispersity is greater than that calculated for the larger AuNP generated on γ-Al_2O_3 and TiO_2 P25, respectively. It is important to note that the detection of AuNP on TiO_2 P25 is difficult due to low contrast and overlap in the NP and support particle size [31].

The supported NP generated using the photochemical method are slightly larger than those formed using the more conventional methods; however there is a distinct difference in controlling parameters between catalytic and photocatalytic processes, with small NP diameter being more important in typical catalytic reactions than in light-activated mechanisms [10]. Recently, light driven synthesis of silver nanoparticles on AgCl illustrated similar size distributions to the supported AuNP presented in this work, with the NP size being on the order of 30–150 nm [32]. Interestingly, these larger particles were shown to be efficient photocatalysts, oxidizing methylic orange dyes in the presence of visible light. In another report, AuNP supported on TiO_2 with average sizes larger than 50 nm have also been employed as efficient photocatalysts for alcohol oxidations [33] and phenol degradation [34]. Further, the use of larger supported AuNP has been proposed to be more useful for pollution control and low temperature combustion as compared to similar marterials of smaller diameter [34]. A recent report by Stamplecoskie et al. also illustrates the applications of larger AgNP, with larger SERS optimal enhancement being observed for particles around 50 nm in diameter [35].

3.3. Effect of % Au loading on particle size

The effects of % wt Au loading on the size of the resultant supported AuNP were also considered. SEM images of a nominal Au loading of 1 wt% and 5 wt% on the three supports of interest were taken to determine the influence of higher gold concentration on the properties of the AuNP composites. Table 1 presents the average size of the AuNP (as determined by SEM) and the nominal Au loadings on HT, γ-Al_2O_3 and TiO_2 P25. The average size of the nanoparticles increases with increasing Au loading, as well as the polydispersity of the nanomaterials. This trend was noted by Galvagno et al. for a series of supported AuNP on metal oxides [36]. Recently, similar results have been noted for AuNP supported on CeO_2 nanopowder [13]. The polydispersity increase on going from 1% to 5% Au loading is well represented by the polydispersity index (PDI) values presented in Table 1. These exploratory results suggest that the concentration of the gold precursor can be employed to control the size of supported AuNP using photochemical nanoparticle synthesis.

3.4. X-ray diffraction spectroscopy

To confirm the presence of metallic gold adsorbed onto the solid supports, samples consisting of a higher loading of 5 wt% Au were prepared. Samples loaded with 1% Au did not display sufficient signal, in agreement with similar studies on clays, where no XRD signal could be observed when the Au loading was ≤2 wt% [37]. The corresponding XRD patterns of 5% Au on HT and 5% Au on γ-Al_2O_3 are presented in Fig. 4. These spectra present the diffraction peaks characteristic for the supports and four additional peaks assigned to Au(1 1 1), Au(2 0 0), Au(2 2 0) and Au(3 1 1) at 38.2°, 44.5°, 64.6° and 77.6°, respectively. Similarly, diffraction peaks due to the four aforementioned Au lattice planes were also observed for 5% Au on TiO_2 P25. These XRD results indicate that metallic gold was readily supported on HT, γ-Al_2O_3 and TiO_2 P25.

3.5. X-ray photoelectron spectroscopy

X-ray photoelectron spectroscopy (XPS) was also used to characterize the oxidation state of the Au species adsorbed on the solid supports (5% Au loading) and, therefore, the gold species responsible for their catalytic activity. Several reports have shown that not only are AuNP effective catalysts for a number of organic reactions, but also ionic gold (i.e., Au^+, Au^{3+}) at the Au-support interface (in the form of metal oxides) [6,38] may also play a major role in the catalytic activity of these materials [5,16,39].

The supported AuNP were thoroughly washed *via* Soxhlet extraction to ensure the removal of Au^{3+} precursor from the support surface prior to use. XPS spectra of 5% Au on γ-Al_2O_3 taken both before and after washing are presented in Fig. 5. A small amount of Au^{3+} was observed prior to washing of the solid, where broadening of the Au^0 peaks was observed at 88.6 eV and 85 eV. Following extensive extraction of the supported materials, no evidence of Au^{3+} was found, indicating that following Soxhlet extraction only metallic gold species remain on the supports. The Au $4f_{5/2}$ peak for Au^0 was readily observed at ~87 eV for the Au on HT nanocomposite, but the corresponding Au $4f_{7/2}$ peak at ~84 eV was unable to be detected due to overlap with the peaks of Mg from the aluminomagnesium solid support used in this system [40]. The Au $4f_{7/2}$ and $4f_{5/2}$ binding energies for Au^0 were observed at 87.5 eV and 83.9 eV, respectively, for both the 5% Au on TiO_2 P25 and γ-Al_2O_3 samples.

4. Exploratory catalytic testing: the reduction of 4-nitrophenolate

Over the past decade, significant effort has been placed on the study of supported AuNP as catalysts in various organic reactions, such as oxidations [5,12,15,17,40,41] and reductions [42–57]. In the case of AuNP, their high surface-to-volume ratio adds to the interest in these nanomaterials as potential catalysts [4]. Supported AuNP from 1–50 nm in size have been shown to be catalytically active, in particular as photocatalysts, towards a variety of organic reactions [10,33,34,55]. The supported AuNP presented in this work fit within this "active" size range, making them good candidates for catalytic testing.

The reduction of nitroarenes has been extensively utilized in the literature for supported Pd [49–51], Ag [42,49,54,56,57] and Au [3,42,43,45–48,52,53,55,56] composites, making this system an attractive reaction for exploratory tests of the catalytic capabilities of supported AuNP. Further, this reaction can be easily followed by UV–visible spectroscopy. In particular, the reduction of 4-nitrophenol to 4-aminophenol in the presence of excess $NaBH_4$

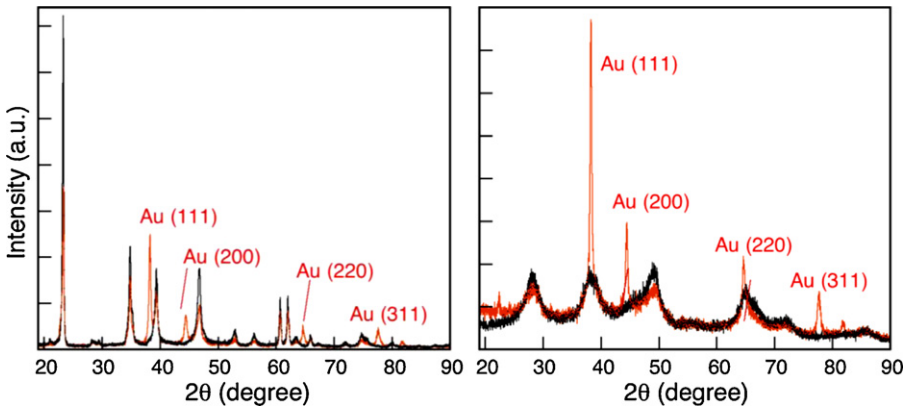

Fig. 4. XRD spectra of 5% Au/HT (left) and 5% Au/γ-Al_2O_3 (right). In these spectra the black trace corresponds to the XRD pattern of the support and the red one to the support plus AuNP.

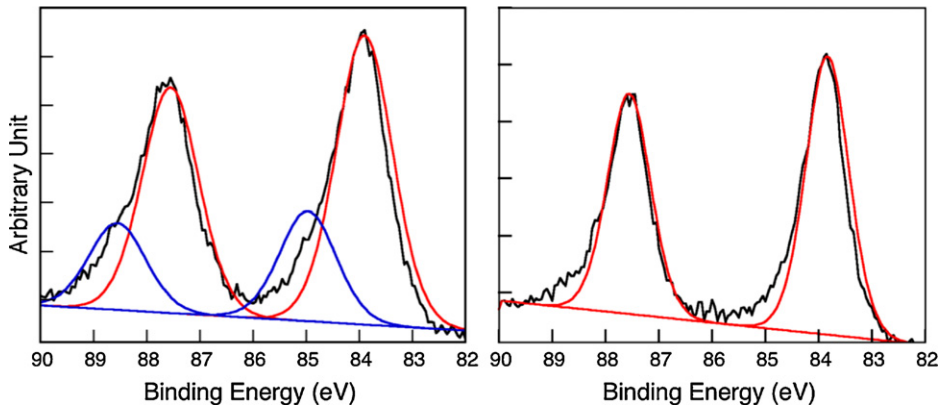

Fig. 5. XPS spectra of 5% Au on γ-Al_2O_3 before (left) and after (right) Soxhlet extraction for 48 h with CH_3CN. The red fits correspond to the deconvoluted binding energies of Au^0 and the blue fits to the deconvoluted binding energies of Au^{3+}. (For interpretation of the references to colour in this figure legend, the reader is referred to the web version of this article.)

has been widely employed to test the catalytic activity of noble metal nanoparticles. The development of novel, greener synthesis of 4-aminophenol is necessary due to its importance in pharmaceutical, industrial and automotive applications [42]. Thus, this system was of preferred choice to examine the performance of our supported AuNP on HT, γ-Al_2O_3 and TiO_2 P25 as potential heterogeneous catalysts.

Upon addition of $NaBH_4$ to a 4-nitrophenol solution, the colour rapidly changed from light to deep yellow. UV–visible spectroscopy illustrated a red-shift in the absorption maximum from 315 nm for the 4-nitrophenol (solution pH = 5) starting material to 400 nm due to the generation of 4-nitrophenolate (4-NO_2) (solution pH = 7) (Fig. 6) [42]. Addition of supported AuNP resulted in a gradual disappearance of the 400 nm band as monitored by UV–visible spectroscopy. The reduction of 4-NO_2 is shown in Fig. 7 with the 400 nm 4-NO_2 absorption band decreasing and giving way to a new species at 290 nm, assigned to 4-aminophenolate (4-NH_2) (solution pH = 8)[42,49,53,55]. No substantial decrease at 400 nm was observed for the three supports studied when control experiments were carried out in the absence of AuNP. These results show that the supported AuNP are catalytically active and that Au is required for this reaction to occur.

The rate constants for the consumption (k_{decay}) of 4-NO_2 at 400 nm were also used to determine the efficiency of the 1% and 5% Au on HT, γ-Al_2O_3 and TiO_2 P25 catalysts in the reduction reaction (Table 2). These values indicate that the % Au loading and the support play an important role in the catalytic ability of these heterogeneous materials. Interestingly, the kinetic decay profile for the 5% Au on TiO_2 P25 revealed a unique induction time for the first 2–3 min of the reaction. This trend has been previously noted in the literature and has been attributed to the presence of O_2 in the aqueous solution, where $NaBH_4$ reacts faster with the excess oxygen than with the 4-NO_2 precursor [42,55] and can also act as a catalyst poison through adsorption onto the NP surface [57]. Purging of the sample with N_2 prior to $NaBH_4$ addition eliminates the

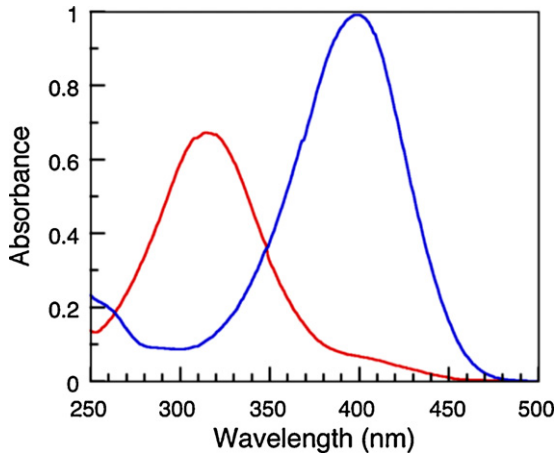

Fig. 6. UV–visible absorption spectra for 4-nitrophenol (red) and 4-nitrophenolate (blue). (For interpretation of the references to colour in this figure legend, the reader is referred to the web version of this article.)

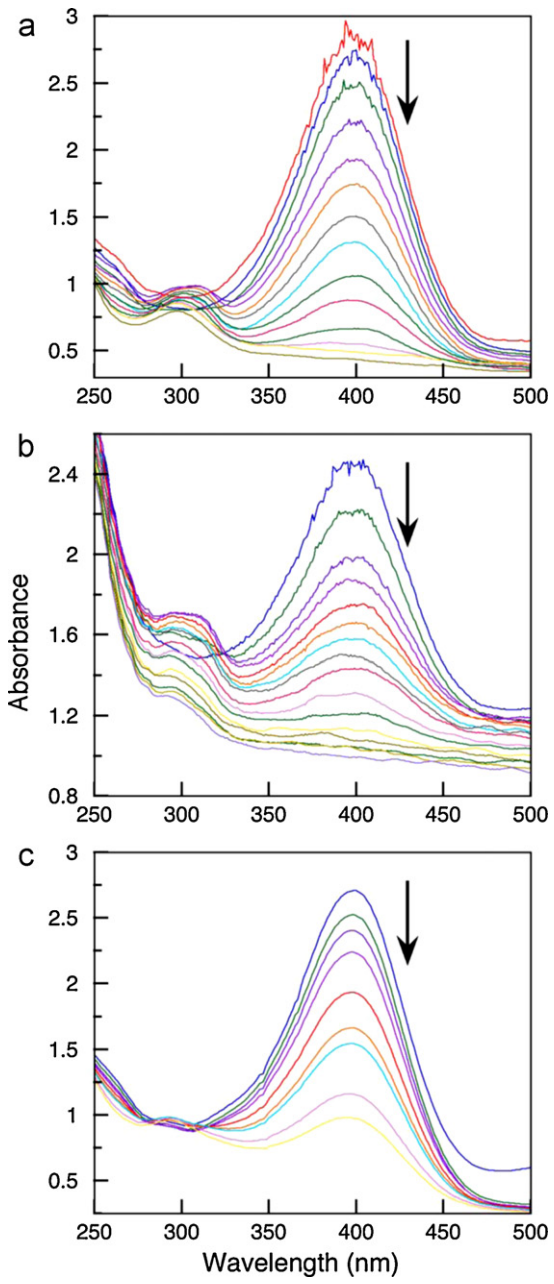

Fig. 7. UV–visible absorption spectra for the reduction of 4-NO_2 catalyzed by: (a) 1% Au on HT, (b) 1% Au on γ-Al_2O_3 and (c) 1% Au on TiO_2 P25.

induction time when using 5% TiO_2 P25 composite, consistent with O_2 inhibition of the catalytic process. The reasoning for the presence of an induction time prior to reduction of 4-NO_2 using 5% Au on TiO_2 P25 is purely speculative and may be related to the large AuNP size increase on varying the composite support from 5% γ-Al_2O_3 to TiO_2. The Au surface area decreases with increasing NP size [55]. As the amount of O_2 in the system can be assumed to remain constant in each trial, the likelihood of adsorption of oxygen onto the low number of catalytically active areas of the 5% TiO_2 P25 composite is increased, resulting in a higher probability of catalyst poisoning. Such an event would require that H_2 first to displace the excess O_2 from the AuNP surface (induction period) to allow for adsorption of the hydrogen and 4-NO_2 precursors and the reduction reaction to proceed.

Table 2
Rate constants for the decay of 4-nitrophenolate using supported AuNP as catalysts.[a]

Support	Au Loading (%)	Ave. NP size (nm)	k_{decay} at 390 nm (min^{-1})	k_{decay}/% Au
HT	1	21	0.6 ± 0.01	0.6
	5	47	2.2 ± 0.2	0.44
γ-Al_2O_3	1	30	0.45 ± 0.01	0.45
	5	112	1.9 ± 0.2	0.38
TiO_2 P25	1	33	0.12 ± 0.05	0.12
	5	142	0.30 ± 0.05	0.06

[a] Values taken at room temperature (23 °C) under air.

4.1. Influence of gold loading

The data in Table 2 show that the % Au loading has a considerable effect on the catalytic activity of supported AuNP and, thus, on the rate of reduction of 4-NO_2. Specifically, on increasing the % Au loading from 1% to 5%, the rate of 4-NO_2 reduction increased for all supports. These results seemed puzzling, as the catalytic activity of AuNP has shown to decrease with increasing AuNP size and NP polydispersity [4–6,55]. The faster consumption of 4-NO_2 when in the presence of the 5% supported Au catalysts may be attributed to the change in the 4-NO_2/mol Au ratio. On varying the Au loading from 1 to 5%, the ratio between the moles of 4-NO_2 and moles of Au was not held constant. Previous studies have shown that the reduction of 4-NO_2 is largely dependant on the amount of catalyst in the solution [55]. Closer examination of the corresponding UV–visible spectra monitored against time for the composites comprising of 5% Au loading (Fig. S12, Supplementary Data) shows that the actual turnover numbers (mol 4-NH_2/% Au loading) as estimated from the top absorption in the UV–visible spectra, are similar or less than that observed for the 1% Au loadings (Fig. 7). For example, λ_{max} at 290 nm is approximately 0.95 for the 1% HT sample and 0.76 for the 5% loading. Furthermore, closer examination of the k_{decay}/% Au values presented in Table 2 reveals that when the amount of adsorbed Au is accounted for, the turnover frequency for the reduction of 4-nitrophenolate is slightly less for the 5% Au composites, as compared to those with 1% Au loading. From these results, it is evident that though the reaction proceeds faster in the presence of the 5% Au loadings, the generation of the product 4-NH_2 is clearly less favourable with these composites.

4.2. Influence of support

The nature of the supports employed in the synthesis of 1% and 5% heterogeneous Au catalysts influences both the catalytic activity of the resultant supported AuNP, but also the ability of the support to chemisorb the 4-nitrophenolate precursor. The support in these solid state materials is known to be an integral participant in catalytic reactions [5,6,16]. One role of the support is to reduce the diffusional mobility of the adsorbed AuNP [5]. However, the support may also be crucial to facilitate adsorption of the 4-nitrophenolate precursor. When considering the point of zero charge (PZC) of the solids chosen for this study, HT has the highest PZC (≈10) [40], followed by γ-Al_2O_3 (PZC = 8) [58] and TiO_2 P25 (PZC ≈ 6)[58]. The PZC of 10 for HT indicates that anions are more favourably adsorbed onto the surface of this support, consistent with this material as an anion exchanged clay. Similarly, the ability of the solid support to effectively bind anionic precursors gradually decreases with increasing PZC. Thus, for the series of supports chosen for this study, HT would bind most favourably the anionic 4-nitrophenolate precursor and TiO_2 P25 the least. The reduced catalytic activity of the 1% and 5% supported AuNP on varying the support from HT, to γ-Al_2O_3 and TiO_2 P25 can also be attributed to reduced affinity for the 4-NO_2 precursor, thereby decreasing the proximity between the starting material and the AuNP catalyst and the rate of 4-NO_2 reduction.

4.3. Catalytic cycling

In order to test the ability of our supported AuNP to cycle in catalysis and also to characterize the AuNP following the reduction of 4-NO_2, the reaction was carried out using the 5% γ-Al_2O_3 AuNP composite due to the ability to image this support with a wide range of techniques. First, the heterogeneous catalyst was analyzed *via* SEM, TEM, XRD and XPS (see Supplementary Data) following use in the reduction of 4-nitrophenolate. SEM analysis showed a fairly consistent particle size of 157 nm average, about 40 nm larger than the value reported prior to catalysis in Table 1. XRD analysis still showed the characteristic diffraction peaks attributed to Au^0 and XPS detected little formation of Au^{3+} during catalysis.

To test the ability of our supported AuNP to cycle, a portion of the 5% γ-Al_2O_3 was cleaned *via* Soxhlet extraction for 48 h to remove any by-products of the reduction reaction that may have been adsorbed onto the AuNP surface. The support was then dried and the reduction of 4-NO_2 carried out as previously described. The resulting k_{decay} of the 4-NO_2 band at 400 nm (presented in Fig. S17) was calculated to be $0.12 \pm 0.07\ min^{-1}$. These results are approximately 16 fold slower than initial catalytic testing, suggesting that while these supported AuNP may be appropriate for many cycles of catalysis, some fatigue in the catalytic efficiency should be expected.

5. Conclusions

Supported AuNP were successfully prepared on HT, γ-Al_2O_3 and TiO_2 P25 using a solvent-free photochemical method employing ketyl radicals as reducing agents; this method involves the irradiation of solid samples under ambient conditions in an inexpensive home-built setup. The % Au loading was varied from 1% to 5%, with the 5% Au loadings forming larger AuNP. The heterogeneous AuNP composites were characterized through various techniques, including diffuse reflectance spectroscopy, SEM and TEM imaging, XRD and XPS and all show the presence of AuNP on the surface of the supports. Further, XPS was used to verify the oxidation state of the adsorbed Au species and concluded that, following Soxhlet extraction, only Au^0 remained on the support surface. The catalytic activity of the series of 1% and 5% Au supports were screened using the reduction of 4-nitrophenolate due to ability to easily monitor the reaction by UV–visible spectroscopy. The results of the screening showed that 4-NO_2 was readily reduced in all cases where the supported AuNP were present. Further, the rate constants for the decay of the 4-NO_2 at 400 nm showed that both the % Au loading and support play an integral role in the efficiency of the AuNP catalyzed reduction reaction. Noteably, this method of generating supported AuNP is environmentally benign by using light as one of the major reagents and by reducing solvent use. These nanomaterials may also prove useful in the field of photocatalysis, where nanoparticle size is not as dominant a factor in dictating the catalytic activity of these particles.

Acknowledgements

We thank the Natural Sciences and Engineering Research Council of Canada and the Canadian Foundation for Innovation for generous support. We also acknowledge Dr. Tara Kell (XRD), Dr. Yun Liu (SEM/TEM) and Dr. Sander Mommers (XPS) for their helpful discussions and help in the imaging of supported AuNP, as well as Dr. Hermenegildo García (Universidad Politécnica de Valencia) for helpful suggestions throughout this work.

Appendix A. Supplementary data

SEM and TEM images, size distribution histograms, XRD, UV–visible spectra (in the absence of AuNP) and time-resolved kinetics (1% and 5% Au loading) for the reduction of 4-NO_2, calculation of PDI.

Supplementary data associated with this article can be found, in the online version, at doi:10.1016/j.jphotochem.2011.08.013.

References

[1] P.K. Jain, I.H. El-Sayed, M.A. El-Sayed, Au nanoparticles target cancer, Nanotoday 2 (2007) 18–29.
[2] J. Zhu, B.M. Lines, M.D. Ganton, M.A. Kerr, M.S. Workentin, Efficient Synethsis of isoxazolidine-tethered monolayer-protected gold nanoparticles (MPGNs) via 1,3-dipolar cycloadditons under high pressure conditions, J. Org. Chem. 73 (2008) 1099–1105.
[3] C. Burda, X. Chen, R. Narayanan, M.A. El-Sayed, Chemistry and properties of nanocrystals of different shapes, Chem. Rev. 105 (2005) 1025–1102.
[4] J.M. Campelo, D. Luna, R. Luque, J.M. Marinas, A.A. Romero, Sustainable preparation of supported metal nanoparticles and their applications in catalysis, ChemSusChem 2 (2009) 18–45.
[5] A. Corma, H. Garcia, Supported gold nanoparticles as catalysts for organic reactions, Chem. Soc. Rev. 37 (2008) 2096–2126.
[6] M. Haruta, Catalysis of gold nanoparticles deposited on metal oxides, Cattech 6 (2002) 102–115.
[7] G.J. Hutchings, M. Brust, H. Schmidbaur, Gold – an introductory perspective, Chem. Soc. Rev. 37 (2008) 1759–1765.
[8] A. Corma, R. Juarez, M. Boronat, F. Sanchez, M. Iglesias, H. Garcia, Gold catalyzes the Sonogashira coupling reaction without the requirement of palladium impurities, Chem. Commun. 47 (2011) 1446–1448.
[9] S. Carretin, Y. Hao, V. Aguilar-Guerrero, B.C. Gates, S. Trasobares, J.J. Calvino, A. Corma, Increasing the number of oxygen vacancies on TiO_2 by doping with iron increases the activity of supported Au for CO oxidation, Chem. Eur. J. 13 (2007) 7771–7779.
[10] A. Primo, A. Corma, H. García, Titania supported gold nanoparticles as photocatalysts, Phys. Chem. Chem. Phys. 13 (2011) 896–910.
[11] B.F.G. Johnson, Nanoparticles in catalysis, Top. Catal. 24 (2003) 147–159.
[12] M. Haruta, T. Kobayashi, H. Sano, N. Yamada, Novel gold catalysts for the oxidation of carbon monoxide at a temperature far below 0 °C, Chem. Lett. 16 (1987) 405–408.
[13] A. Abad, A. Corma, H. Garcia, Catalysts parameters determining activity and selectivity of supported gold nanoparticles for the aerobic oxidation of alcohols: the molecular reaction mechanism, Chem. Eur. J. 14 (2008) 212–222.
[14] W. Fang, Q. Zhang, J. Chen, W. Deng, Y. Wang, Gold nanoparticles on hydrotalcite as efficient catalysts for oxidant-free dehydrogenation of alcohols, Chem. Commun. 46 (2010) 1547–1549.
[15] T. Mitsudome, A. Noujima, T. Mizugaki, K. Jitsukawa, K. Kaneda, Efficient aerobic oxidation of alcohols using a hydrotalcite supported gold nanopartile catalyst, Adv. Synth. Catal. 351 (2009) 1890–1896.
[16] V.R. Choudhary, D.K. Dumbre, Supported nano-gold catalysts for epoxidations of styrene and oxidation of benzyl alcohol to benzaldehyde, Top. Catal. 52 (2009) 1677–1687.
[17] A. Abad, A. Corma, H. Garcia, Supported gold nanoparticles for aerobic, solventless oxidation of allylic alcohols, Pure Appl. Chem. 79 (2007) 1847–1854.
[18] Y.J. Chen, C. Yeh, Deposition of highly dispersed gold on alumina support, J. Catal. 200 (2001) 59–68.
[19] M.L. Marin, K.L. McGilvray, J.C. Scaiano, Photochemical strategies for the synthesis of gold nanoparticles from Au(III) and Au(I) using photoinduced free radical generation, J. Am. Chem. Soc. 130 (2008) 16572–16584.
[20] K.L. McGilvray, M.R. Decan, D. Wang, J.C. Scaiano, Facile photochemical synthesis of unprotected aqueous gold nanoparticles, J. Am. Chem. Soc. 128 (2006) 15980–15981.
[21] J.C. Scaiano, P. Billone, C.M. Gonzalez, L. Maretti, M.L. Marin, K.L. McGilvray, N. Yuan, Photochemical routes to silver and gold nanoparticles, Pure Appl. Chem. 81 (2009) 635–647.
[22] C.M. Gonzalez, Y. Liu, J.C. Scaiano, Photochemical strategies for the facile synthesis of gold–silver alloy and core–shell bimetallic nanoparticles, J. Phys. Chem. C 113 (2009) 11861–11867.
[23] K. Zeitler, Photoredox catalysis with visible light, Angew. Chem. Int. Ed. 48 (2009) 9785–9789.
[24] P. Quaresma, L. Soares, L. Contar, A. Miranda, I. Osório, P.A. Carvalho, R. Franco, E. Pereira, Green photocatalytic synthesis of stable Au and Ag nanoparticles, Green Chem. 11 (2009) 1889–1893.
[25] S. Eustis, M.A. El-Sayed, Why gold nanoparticles are more precious than pretty gold: noble metal surface plasmon resonance and its enhancement of the radiative and nonradiative properties of nanocrystals of different shapes, Chem. Soc. Rev. 35 (2006) 209–217.
[26] G. Mie, Beitrage zur optik trüber medien, speziell kolloidaler metallösugun, Ann. Phys. 25 (1908) 377–445.
[27] M. Torrell, R. Kabir, L. Cunha, M.I. Vasilevskiy, F. Vaz, A. Carvalerio, E. Alves, N.P. Barradas, Tuning of surface plasmon resonance in TiO_2/Au thin films grown by magnetron sputtering: the effect of thermal annealing, J. Appl. Phys. 109 (2011) 07431(0)–07431(9).
[28] P.V. Kamat, Photophysical, photochemical and photocatalytic aspects of metal nanoparticles, J. Phys. Chem. B 106 (2002) 7729–7774.
[29] D.A. Skoog, F.J. Holler, T.A. Nieman, Principles of Instrumental Analysis, Fifth ed., Harcourt Brace & Company, Orlando, FL, 1998.

[30] H.P.R. Frederikse, Permittivity (dielectric constant) of inorganic solids, in: W.M. Haynes (Ed.), CRC Handbook of Chemistry and Physics, 91st Edition (Internet Version), CRC Press/Taylor, Boca Raton, FL, 2011.
[31] S. Scire, C. Crisafulli, S. Guiffrida, C. Mazza, P.M. Riccobene, A. Pistone, G. Ventimiglia, C. Bongiorno, C. Spinella, Supported silver catalysts prepared by depostion in aqueous solution of Ag nanoparticles obtained through a photochemical approach, Appl. Catal. A: Gen. 367 (2009) 138–145.
[32] P. Wang, B. Huang, X. Qin, X. Zhang, Y. Dai, J. Wei, M.H. Whangbo, AgAgCl. A highly efficient and stable photocatalyst active under visible light, Angew. Chem. Int. Ed. 47 (2008) 7931–7933.
[33] E. Kowalska, O.O.P. Mahaney, R. Abe, B. Ohtani, Visible-light induced photocatalysis through the surface plasmon excitation of gold on titania surfaces, Phys. Chem. Chem. Phys. 12 (2010) 2344–2355.
[34] A. Zielinska-Jurek, E. Kowalska, J.W. Sobczak, W. Lisowski, B. Ohtani, A. Zaleska, Preparation and characterization of monometallic Au and bimetallic Ag/Au modified-titania photocatalysts activated by visible light, Appl. Catal. B: Environ. 101 (2011) 504–514.
[35] K.G. Stamplecoskie, J.C. Scaiano, V.S. Tiwari, H. Anis, Optimal size of silver nanoparticles for surface enhanced Raman spectroscopy, J. Phys. Chem. C 115 (2011) 1403–1409.
[36] S. Galvagno, G. Parravano, Chemical reactivity of supported gold, J. Catal. 55 (1978) 178–190.
[37] L. Zhu, S. Lataief, Y. Liu, F. Gervais, C. Detellier, Clay mineral supported gold nanoparticles, Appl. Clay Sci. 43 (2009) 439–446.
[38] L. Fu, N.Q. Wu, J.H. Yang, F. Qu, D.L. Johnson, M.C. Kung, H.H. Kung, V.P. Dravid, Direct evidence of oxidized gold on supported gold catalysts, J. Phys. Chem. B 109 (2005) 3704–3706.
[39] L. Wang, Y. Shen, M. Jia, B. Zhaorigetu, The influence of pH on the nano Au/Y catalyst activity for CO oxidation, React. Kinet. Catal. Lett. 97 (2009) 125–130.
[40] C.T. Chang, B.J. Liaw, C.T. Huang, Y.Z. Chen, Preparation of Au/Mg_xAlO hydrotalcite catalysts for CO oxidation, Appl. Catal. A: Gen. 332 (2007) 216–224.
[41] Y.M. Kang, B.Z. Wan, Preparation of gold in Y type zeolite for carbon monoxide oxidation, Appl. Catal. A: Gen. 128 (1995) 53–60.
[42] S. Saha, A. Pal, S. Kundu, S. Basu, T. Pal, Photochemical green synthesis of calcium-alginate-stabilized Ag and Au NPs and their catalytic application to 4-nitrophenol reduction, Langmuir 26 (2010) 2885–2893.
[43] A. Corma, P. Serna, Chemoselective hydrogenation of nitro compounds with supported gold catalysts, Science 313 (2006) 332–334.
[44] W.Y. Ahn, S.A. Sheeley, T. Rajh, D.M. Cropek, Photocatalytic reduction of 4-nitrophenol with arginine-modified titanium dioxide nanoparticles, Appl. Catal. B: Environ. 74 (2007) 103–110.
[45] M. Boronat, P. Concepcion, A. Corma, S. Gonzalez, F. Illas, P. Serna, A molecular mechanism for the chemoselective hydrogenation of substituted nitroaromatics with nanoparticles of Au on TiO_2 catalysts: a cooperative effect between Au and the support, J. Am. Chem. Soc. 129 (2007) 16230–16237.
[46] M. Boronat, F. Illas, A. Corma, Active sites for H_2 adsorption and activation in Au/TiO_2 and the role of the support, J. Phys. Chem. A 113 (2009) 3750–3757.
[47] F. Cardenas-Lizana, S. Gomez-Quero, M.A. Keane, Exclusive production of chloroaniline from chloronitrobenzene over Au/TiO_2 and Au/Al_2O_3, ChemSusChem 1 (2008) 215–221.
[48] Y.C. Chang, D.H. Chen, Catalytic reduction of 4-nitrophenol by magnetically recoverable Au nanocatayst, J. Hazard. Mater. 165 (2009) 664–669.
[49] K. Esumi, R. Isono, T. Yoshimura, Preparation of PAMAM- and PPI-metal (Ag, Pt, and Pd) nanocomposites and their catalytic activities for reduction of 4-nitrophenol, Langmuir 2004 (2004) 237–243.
[50] S.K. Ghosh, M. Mandal, S. Kundu, S. Nath, T. Pal, Bimetallic Pt-Ni nanoparticles can catalyse the reduction of aromatic nitro compounds by $NaBH_4$ in aqueous solution, Appl. Catal. A: Gen. 268 (2004) 61–66.
[51] S. Harish, J. Mathiyarasu, K.L.N. Phani, V. Yegnaraman, Synthesis of conducting polymer supported Pd nanoparticles in aqueous medium and catalytic activity towards 4-nitrophenol reduction, Catal. Lett. 128 (2009) 197–202.
[52] K. Hayakawa, T. Yoshimura, K. Esumi, Preparation of Au-dendrimer nanocomposites by laser irradiation and their catalytic reduction of 4-nitrophenol, Langmuir 19 (2003) 5517–5521.
[53] J. Lee, J.C. Park, J.U. Bang, H. Song, Precise tuning of porosity and surface functionality in Au@SiO_2 nanoreactors for high catalytic efficiency, Chem. Mater. 20 (2008) 5839–5844.
[54] Y. Lu, Y. Mei, M. Drechsler, M. Ballauff, Thermosensitive core-shell particles as carriers for Ag nanoparticles: modulating the catalytic activity by a phase transition in networks, Angew. Chem. Int. Ed. 45 (2006) 813–816.
[55] S. Panigrahi, S. Basu, S. Praharaj, S. Pande, S. Jana, A. Pal, S.K. Ghosh, T. Pal, Synthesis and size-selective catalysis by supported gold nanoparticles: study on heterogeneous and homogeneous catalytic processes, J. Phys. Chem. C 111 (2007) 4596–4605.
[56] N. Pradhan, A. Pal, T. Pal, Catalytic reduction of aromatic nitro compounds by coinage metal nanoparticles, Langmuir 17 (2001) 1800–1802.
[57] N. Pradhan, A. Pal, T. Pal, Silver nanoparticle catalyzed reduction of aromatic nitro compounds, Colloids Surf. A 196 (2002) 247–257.
[58] F. Pinna, Supported metal catalyst preparation, Catal. Today 41 (1998) 129–137.